Raman study of $AlPO_4$ (berlinite) at the α–β transition

2003 J. Phys.: Condens. Matter 15 4487

(http://iopscience.iop.org/0953-8984/15/25/316)

INSTITUTE OF PHYSICS PUBLISHING JOURNAL OF PHYSICS: CONDENSED MATTER

J. Phys.: Condens. Matter **15** (2003) 4487–4501 PII: S0953-8984(03)61727-3

Raman study of $AlPO_4$ (berlinite) at the α–β transition

I Gregora[1], N Magneron[2,4], P Simon[2], Y Luspin[2], N Raimboux[2] and E Philippot[3]

[1] Institute of Physics, ASCR, 18212 Prague 8, Czech Republic
[2] CRMHT–CNRS, 45071 Orléans Cedex 2, France
[3] LPMC–CNRS, 34095 Montpellier, France

E-mail: gregora@fzu.cz

Received 2 April 2003
Published 13 June 2003
Online at stacks.iop.org/JPhysCM/15/4487

Abstract

The A_1-symmetry Raman spectra of berlinite in a broad temperature range, encompassing the α–β phase transition, are reported. The temperature dependence of the lattice mode parameters is presented, particularly concerning the 'soft' mode at $\sim$220 cm^{-1}, which exhibits a complex behaviour in the α phase. This is accounted for by coupling with another A_1 mode and two-phonon background in the α phase. It is shown that the soft-mode parameters do not show appreciable discontinuities at the transition. The fact that four Raman active A_1 modes instead of three are observed in the hexagonal β phase can be understood by assuming a dynamical disorder of Al and P atoms over trigonal α-phase sites.

1. Introduction

Aluminium phosphate $AlPO_4$ is isomorphous to SiO_2. Its stable form at normal temperature and pressure is berlinite (quartzlike structure). On heating, it undergoes the same sequence of transitions: α-quartz $\rightarrow$ β-quartz, α-tridymite $\rightarrow$ β-tridymite and α-cristobalite $\rightarrow$ β-cristobalite [1]. All these polymorphic forms of $AlPO_4$ consist in alternate succession of $(AlO_4)^{5-}$ and $(PO_4)^{3-}$ tetrahedra. The displacive phase transition near 860 K from the low-temperature α-quartz phase (space group $P3_121$ or $P3_221$) to the high-temperature β-quartz phase ($P6_422$ or $P6_122$) was identified a long time ago [2]. In the early 1980s, it was shown that from 857 to 860 K an incommensurate order appears in the system between the α and β phase, in a slightly broader temperature interval than in quartz [3–5].

At room temperature and pressure, vibrational properties of $AlPO_4$ have been investigated by infrared [6–11], Raman scattering [6, 7, 12, 13] and inelastic neutron scattering [14], as well as lattice-dynamical model calculations [7, 15, 16]. Pressure dependence and anharmonicity of Raman phonons were studied at low temperatures [17]; high-pressure Raman spectra were

[4] Now at IUFM, F-45044 Orléans Cedex 1, France.

also reported [18, 19] and studied by model simulations [20, 21]. Recently, the temperature dependence of the crystal structure of $AlPO_4$ was investigated by x-ray diffraction [22–24] and by molecular dynamics simulation [25]. The available results seem to indicate that the α–β transition in $AlPO_4$ is analogous to that in SiO_2.

However, apart from a short communication [26] from the 1970s, no detailed study of the behaviour of optical phonons in $AlPO_4$ over a broad temperature range has been reported. Although the results reported in [26, 27] are taken as strong evidence in favour of a close similarity between the soft-mode behaviour in $AlPO_4$ and SiO_2, the underlying experimental data are too crude to provide convincing conclusions.

We have recently studied the temperature behaviour of $AlPO_4$ by Brillouin scattering and infrared reflectivity/emissivity spectroscopy [28–30]. In the present paper, we report new results of detailed Raman scattering investigations in $AlPO_4$ over the temperature range of 300–1100 K, which encompasses the α–β transition. The emphasis is on the behaviour of the fully symmetric A_1 modes. No special attention is paid to the narrow interval of incommensurate phase.

2. Crystal-structure data and experimental details

The structure of $AlPO_4$ (berlinite) derives from that of SiO_2 (quartz) by replacing the Si atoms alternately by P and Al atoms, resulting in the doubling of the c-axis parameter. In the trigonal α phase, berlinite corresponds to the space group $P3_121$ (or the enantiomorphic $P3_221$ variety) with three $AlPO_4$ formula units in the primitive hexagonal cell [31]. The room-temperature values of the lattice parameters are $a = b = 4.942$ Å and $c = 10.97$ Å [32, 33]. Above 860 K, the hexagonal β modification is characterized by the space group $P6_422$ (or $P6_222$), with lattice parameters $a = b = 5.040$ Å and $c = 11.062$ Å (at 923 K [24]). Using the conventional basis setting of the hexagonal $P6_422$ group for both phases, the correlation between the Wyckoff positions of atoms is as follows (the fractional coordinates of representative atoms in the hexagonal basis are given in parentheses):

	α phase	β phase
3Al:	$3a(u_1, 0, 0)$	$\leftrightarrow 3c(1/2, 0, 0)$
3P:	$3b(u_2, 0, 1/2)$	$\leftrightarrow 3d(1/2, 0, 1/2)$
12O:	$6c_1(x_1, y_1, z_1) + 6c_2(x_2, y_2, z_2)$	$\leftrightarrow 12k(x, y, z)$.

Geometrically, the structure can be viewed as a 3D network of alternating, very nearly regular AlO_4 and PO_4 tetrahedra linked by common corners. The average tetrahedral P–O bonds (∼1.51 Å) are significantly shorter than Al–O (∼1.72 Å) [24]. A comparative study [16] shows that the PO_4 tetrahedra are considerably more strongly bonded than AlO_4 so that the berlinite structure of $AlPO_4$ should be regarded as a crystal of $(PO_4)^{3-}$ anions linked by Al^{3+} cations, rather than an array of corner-sharing tetrahedra like in quartz SiO_2.

In both α and β phases, the primitive cell contains three $AlPO_4$ units, leading thus to 54 degrees of freedom. The 54 normal vibration modes of the Brillouin zone centre are classified according to the irreducible representations of the corresponding point groups as given in table 1, where the IR and Raman activity is also summarized.

For our measurements, suitably oriented slabs ∼1 mm thick were cut from $AlPO_4$ single crystals grown by the hydrothermal method [34–36] and their faces were polished to optical quality. The samples were colourless, highly transparent and free of inclusions.

Table 1. Correlation and activity of the Γ-point lattice vibration modes (ac.–acoustic, op.–optical) in α and β phases of berlinite structure.

α phase: 32 ($P3_121$ or $P3_221$)			β phase: 622 ($P6_422$ or $P6_222$)	
Activity	Modes ac. + op.	Symmetry	Modes ac. + op.	Activity
Raman ($xx + yy, zz$)	8	A_1	3	Raman ($xx + yy, zz$)
		B_1	5	Silent
IR (z)	1 + 9	A_2	1 + 4	IR (z)
		B_2	5	Silent
IR (x, y); Raman (yz, xz) ($xx - yy, xy$)	1 + 17	E E_1	1 + 9	IR (x, y); Raman (yz, xz)
		E_2	8	Raman ($xx - yy, xy$)

The Raman spectra were recorded with a Jobin–Yvon T64000 spectrometer operating in triple subtractive mode (three 1800 grooves mm^{-1} gratings) and equipped with a liquid-nitrogen cooled CCD detector. The spectral range covered extended from 15 to 1300 cm^{-1} and the resolution was approximately 1.5 cm^{-1}. The 514.5 nm line of an argon–krypton Coherent Innova 70 Spectrum laser was mainly used for excitation, with an incident power of about 40 mW arriving on the sample. Alternatively, some spectra were also taken at the 488 nm excitation. An Olympus confocal optical microscope was used to focus the laser into a $\sim$2 μm sized spot on the sample. As checked by comparing the spectra taken at different laser powers, no measurable local heating effects in the sample were observed at these power densities. To minimize the influence of the surface effects, however, the laser focus was lowered to $\sim$40 μm below the sample surface. All experiments were performed in backscattering geometry with pure A_1 spectra studied mainly in $y(zz)\bar{y}$ configuration. (Porto's notation [37] referring to the standard setting of the Cartesian system for the 32_x point group is used.) For comparison, and to check for possible leakage of strong modes into forbidden geometries due to alignment errors and/or to the finite collection angle of the microscope objective, other configurations were also investigated: E(TO), E(LO) and A_1 + E(TO) in $z(yx)\bar{z}$, $y(xz)\bar{y}$ and $y(xx)\bar{y}$ spectra, respectively. This also enabled us to get semi-quantitative information on the relative strengths of the different components of the Raman tensor.

High-temperature Raman spectra were measured using a Linkam TS 1500 heating stage under the microscope. A Pt thermocouple served as a temperature sensor, with an absolute accuracy of $\pm$1 K over the whole temperature range studied (300–1100 K). In the vicinity of the α–β transition, the spectra were taken at steps as fine as 1 K. Since our Raman data did not show any variations meaningfully reflecting the narrow range of the incommensurate phase, throughout this paper we shall use only one quantity, labelled T_i, to indicate the α–β transition temperature. The relative accuracy of its value, as determined from our spectra, is estimated to $\pm$1 K.

The possible presence of a quasi-elastic scattering component was investigated using a triple-pass plane Fabry–Perot interferometer (effective finesse 70; resolving power 760 000) tuned to the maximum of the Rayleigh peak. The light source was the 514.5 nm line of a single-frequency Ar-ion laser.

3. Results

3.1. Assignment

The overall view of the temperature evolution of the $y(zz)\bar{y}$ Raman spectra of $AlPO_4$ is given in figure 1. The features assigned to A_1 fundamental modes are labelled 1–8 in order of

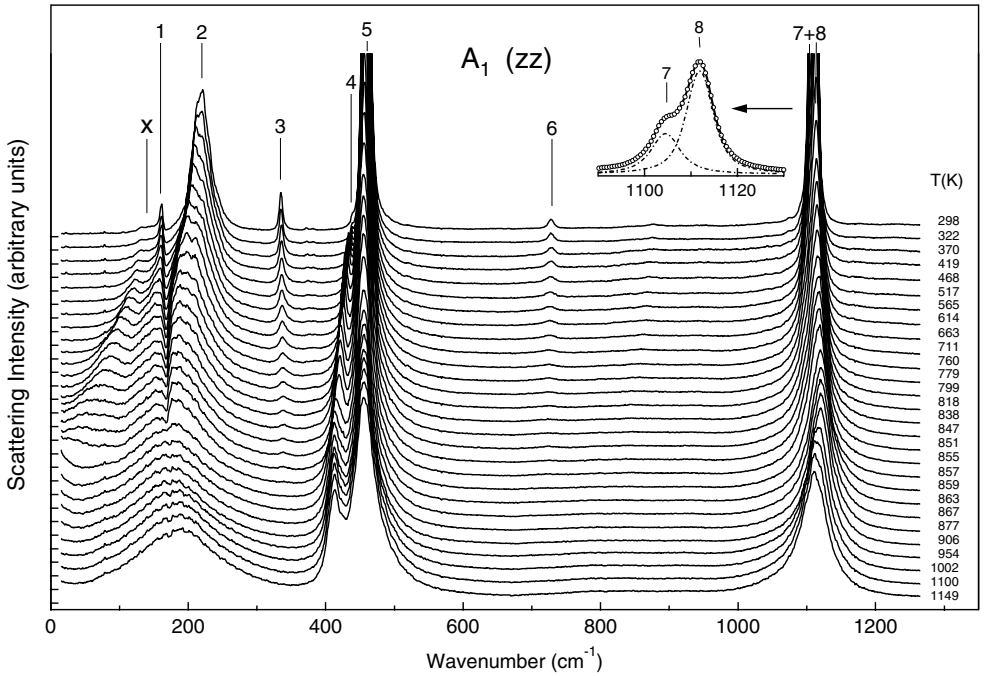

Figure 1. Temperature dependence of $y(zz)\bar{y}$ Raman spectra of $AlPO_4$ (spectra are uncorrected for temperature factors). The eight A_1 modes observed at room temperature are marked by numbered thin curves. An additional soft feature is marked by x. The two-component structure of the 7 + 8 band at room temperature is shown in the inset.

increasing frequency. An additional low-frequency feature at $\sim$140 cm^{-1} (room-temperature value) is marked by 'x'.

Our room-temperature results agree well with those previously obtained [12, 13]: eight A_1 vibration modes—predicted by the group theory for the α phase—can be identified in the spectra at temperatures below $T_i \sim 860$ K. The spectrum is dominated by three strong bands (labelled 2, 5 and 8) located at 221, 461 and 1112 cm^{-1}. These modes correspond to the A_1 zone-centre modes of quartz (α-SiO_2). The remaining five weaker A_1 modes (1, 3, 4, 6 and 7), located at 162, 336, 439, 728 and 1104 cm^{-1}, respectively, derive from the zone-boundary modes in the A point of the α-SiO_2 Brillouin zone, due to the folding of phonon branches along the c^* direction.

Disregarding slight differences in the frequency values, our assignment of all the eight A_1 modes is in full agreement with the most recent polarized Raman studies [13]. Comparison of the room-temperature spectra at different polarization configurations unambiguously excludes the earlier assignment [6, 7, 38] of the high-frequency A_1 modes. In particular, the lower-frequency component of the A_1 doublet 7 + 8 in the zz spectra is clearly no leakage of a strong E(LO) mode at nearly the same frequency. We note also that this 1104 cm^{-1} A_1 component has vanishing strength in the xx spectra. In contrast, the A_1 mode 4 at 439 cm^{-1}—undetected in [6] and [12] because of masking by an E mode of a very close frequency—has negligible strength in zz but large in xx, where it is comparable to the A_1 mode 5 at 461 cm^{-1}.

The 'extra' A_1 feature at $\sim$140 cm^{-1}, well known from earlier Raman studies, is barely discernible at room temperature. With increasing temperature, however, its intensity markedly grows while its frequency drops down, until it disappears in the Rayleigh wing on approaching the phase transition.

3.2. The fitting procedure

In the endeavour to obtain quantitative information from our spectra, we performed extensive fitting of our data. While most of the peaks can be very well modelled with independent damped harmonic oscillators, the two lowest A_1 modes (1 and 2) show clear indication of coupling, with a pronounced asymmetry and a deep anti-resonance minimum in between. The coupling is obvious even in the room-temperature spectra. Up to about 500 K, the band shape shows some additional structure in the form of weak shoulders, in particular on the upper of the two coupled modes. Hence, to extract the peak parameters from the spectra throughout the whole temperature range studied, we applied a multi-peak fit combining independent damped (quasi-harmonic) oscillators with a coupled damped harmonic oscillator (CDHO) pair—with coupling introduced between the modes 1 and 2. No satisfactory fit to the coupled line shape could be made with two independent oscillators up to the phase transition temperature ~860 K. On the other hand, the independent oscillator fit was adequate at higher temperatures.

Rather than correcting the spectra for the temperature factor prior to fitting, we preferred to include this factor in the fitting function, since this enabled us to use a similar background function at all temperatures and, possibly, different thermal factors for different features. For example, the weak parasitic plasma lines from the laser could be included in the fit as narrow Gaussians serving as convenient frequency markers.

The first-order (Stokes) Raman response $R(\omega)$ for two coupled damped quasi-harmonic modes was fitted using the following well known mode-coupling formula (see, e.g. [39, 40]):

$$R(\omega) = -\operatorname{Im}(\tilde{\boldsymbol{f}} \cdot \boldsymbol{T}(\omega) \cdot \boldsymbol{f}) \cdot (1 + n(\omega, T)),$$

with

$$\boldsymbol{T}^{-1}(\omega) = \begin{pmatrix} \omega_1^2 - \omega^2 + \mathrm{i}\gamma_1\omega & \Delta_{12} \\ \Delta_{12} & \omega_2^2 - \omega^2 + \mathrm{i}\gamma_2\omega \end{pmatrix},$$

$$\boldsymbol{f} = \begin{pmatrix} f_1 \\ f_2 \end{pmatrix} \qquad \text{and} \qquad n(\omega, T) = (\exp(\hbar\omega/kT) - 1)^{-1}.$$

The Raman mode-strength parameter $f_j = (\partial\chi/\partial u_j)$ corresponds to the susceptibility derivative with respect to the jth bare normal mode u_j of eigenfrequency ω_j and damping γ_j. We note that for vanishing coupling ($\Delta_{12} \to 0$) the Raman response $R(\omega)$ goes over to the usual sum of independent contributions

$$R(\omega) \cong (1 + n(\omega, T)) \sum_j |f_j|^2 \frac{\gamma_j\omega}{(\omega_j^2 - \omega^2)^2 + \mathrm{i}\omega\gamma_j}$$

and the integrated Raman intensities of individual modes (without the thermal factor) are given by $S_j \cong \pi|f_j|^2/2\omega_j$ as long as their damping is not too strong ($\gamma_j \ll \omega_j$).

Our choice was that of a real coupling parameter Δ_{12}. To fix the sign ambiguity in the parameter set—due to a mixed term $\sim f_1 f_2 \Delta_{12}$ in the explicit expression for $R(\omega)$—we constrained the fit by requiring f_1 and f_2 be non-negative. We checked that an equally good fit to the data with imaginary coupling term $\mathrm{i}\omega\Gamma_{12}$ (corresponding to a different choice of phase [38]) was always possible, yielding somewhat differently renormalized values of the bare mode parameters. The main difference was the opposite behaviour of the coupling parameters with increasing temperature: whereas Δ_{12} decreased, Γ_{12} increased.

As an example, we show in figure 2(a) the CDHO fit of the low-frequency part of the $A_1(zz)$ Raman spectrum at room temperature: the 'extra' feature x and additional shoulders c on the coupled mode line shape were fitted by Gaussians. For comparison, the two lowest E(TO) modes observed in $z(yx)\bar{z}$ configuration and fitted with independent oscillators are shown in figure 2(b). An example of the fits to the low-frequency $A_1(zz)$ spectra at two high temperatures, below and above T_i, is shown in figure 3.

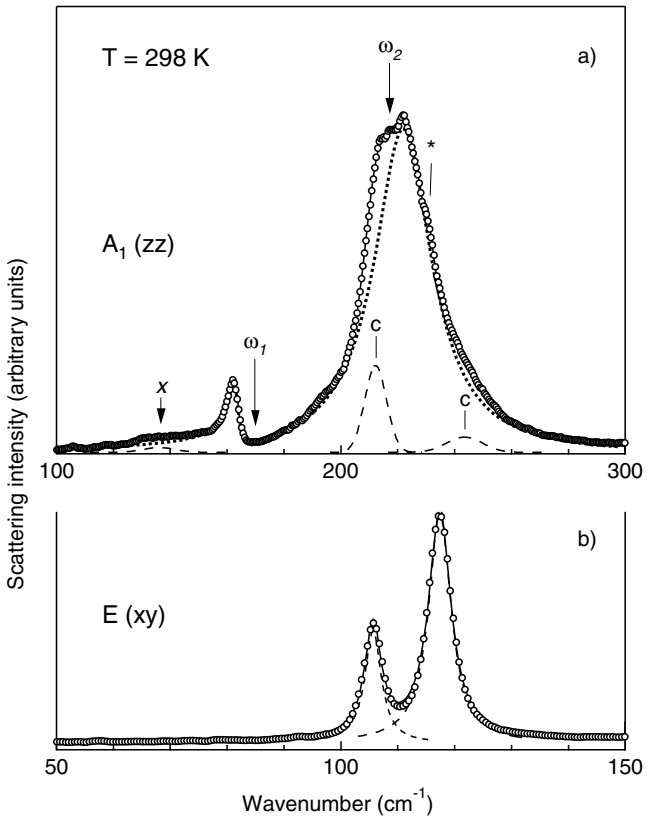

Figure 2. (a) A coupled oscillator fit to the low-frequency part of the $y(zz)\bar{y}$ spectrum at $T = 298$ K: open circles—experimental data, solid curve—fit, dotted curve—coupled curve shape, dashed curves—additional components. Arrows mark the location of the decoupled frequencies ω_1 and ω_2 corresponding to modes 1 and 2 and of the soft feature (x). Two components c represent fine structure on the coupled line shape (* marks a laser plasma line). (b) Oscillator fit to $z(yx)\bar{z}$ spectra at $T = 298$ K, showing the two lowest E(TO) modes at 106 and 117 cm^{-1}. The wavenumber scale is twice expanded with respect to (a).

3.3. Temperature dependence of A_1 Raman spectra

Figures 4(a)–(d) summarize the temperature dependence of the peak parameters (as obtained from our fits to the spectra in the temperature range of 300–1150 K, comprising the $\alpha \rightarrow \beta$ phase transitions in the neighbourhood of 857–860 K.

The general behaviour is qualitatively similar to that observed in quartz [41, 42]. All A_1 modes broaden with increasing temperature and show more or less conspicuous anomalies at the phase transition. Modes 1, 3, 6 and 7 become progressively weaker and virtually disappear on approaching $T_i = 860$ K. The remaining four modes, 2, 4, 5 and 8, clearly persist in the β phase. Their oscillator parameters also show virtually continuous variation with temperature. Close to the phase transition, the damping parameter of these four modes shows characteristic behaviour, very similar to the 'infrared damping divergences' observed in quartz [43, 44]—see figure 4(b).

The two highest-frequency peaks, 7 and 8, are components of a closely spaced doublet, barely resolved at room temperature. With increasing temperature, they broaden and merge into

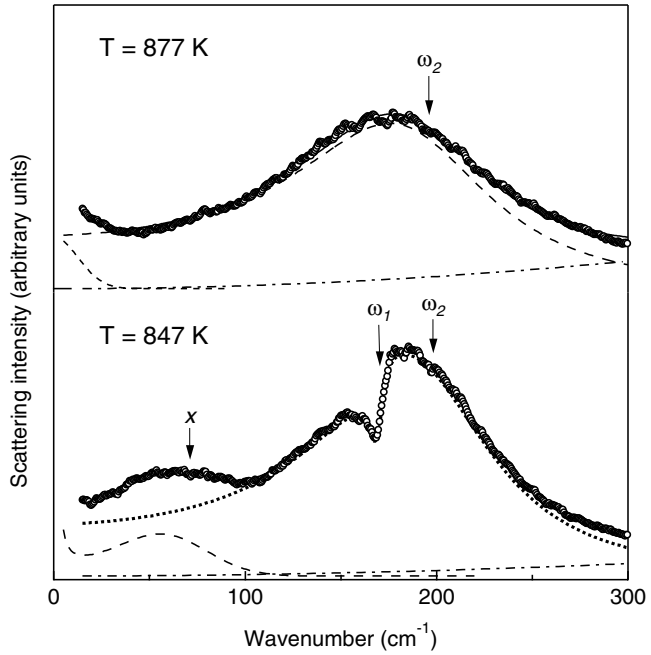

Figure 3. Fit to the low-frequency part of the $y(zz)\bar{y}$ spectra below (847 K) and above (877 K) the α–β phase transition (T_i = 860 K): dotted curve—coupled curve shape, dashed curve—independent peaks, dot-and-dashed curve—baseline. The increased intensity below 30 cm^{-1} in the β phase (877 K) is modelled by a 'central' Gaussian component. Arrows mark the decoupled frequencies ω_1 and ω_2 corresponding to modes 1 and 2, and of the soft feature x (second-order Gaussian).

a single peak whose band shape, however, remains asymmetric up to the transition temperature. The parameters of both individual components of the unresolved doublet below T_i are not determined unambiguously and hence no special significance should be given to the details of their temperature dependences below T_i, in particular to the strength (see figure 4(c)). More significant is the total effective strength of the doublet (7 + 8), derived from the sum of integrated intensities, which shows a reasonably smooth behaviour throughout the whole temperature range. It is nonetheless clear from the fits that the lower mode (7) vanishes at T_i and the total strength of the doublet is taken over by the upper mode (8), which slightly hardens on heating (figure 4(a)).

A different behaviour is observed for the two close peaks 4 and 5 at 437 and 461 cm^{-1}. The lower mode is observed only as a very weak shoulder at low temperatures. On heating, however, its strength markedly grows with temperature at the expense of the upper mode. It shows also appreciable softening on approach to T_i, whereas the 461 cm^{-1} peak frequency is practically unaffected. The sum of the integrated intensities of both peaks, hence also the total effective strength of the pair, depends again very little on temperature. The 461 cm^{-1} peak shows slight but noticeable asymmetric broadening towards higher frequencies at all temperatures.

The two low-frequency A_1 modes 1 and 2 are strongly coupled all the way up to T_i. As shown in figure 4(a), the decoupled (bare) frequency ω_2 of the upper mode only very slightly softens with increasing temperature—from 211 cm^{-1} down to about 200 cm^{-1} near T_i—while its bare damping γ_2 markedly increases. The lower peak shows quite a low bare damping,

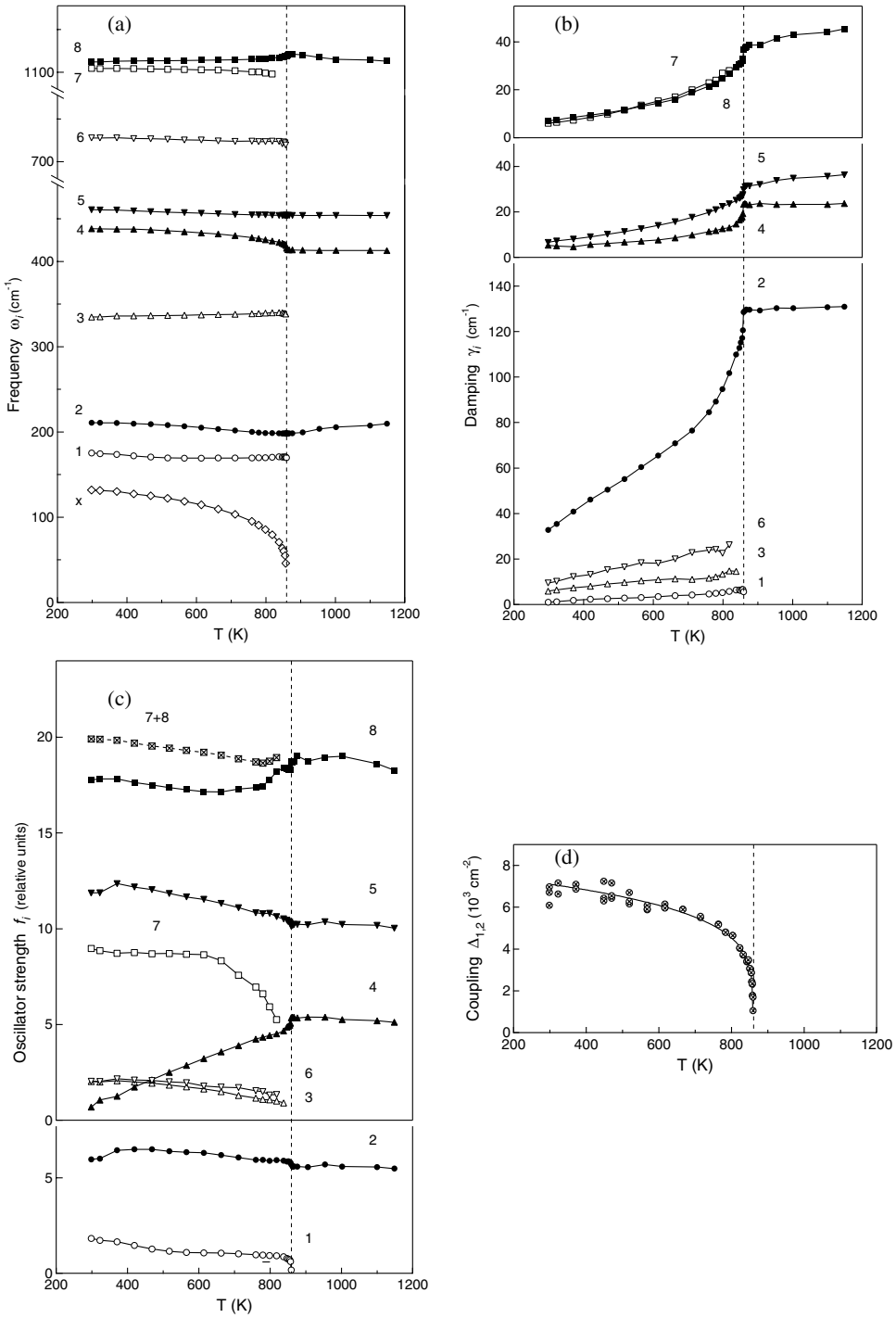

Figure 4. Temperature dependence of the A_1 oscillator parameters. Solid curves are guides to the eye. The phase transition temperature, $T_i = 860$ K, is marked by a dashed vertical line. (a) Frequencies (including that of the low-frequency soft feature x). (b) Damping parameters (FWHM). (c) Mode strengths. The total effective strength of the 7 + 8 doublet below T_i is also plotted. (d) Coupling parameter Δ_{12} between modes 1 and 2.

$\gamma_1 < 5$ cm^{-1}, all the way up to T_i (figure 3(b)), and its bare frequency (decoupled value $\omega_1 \sim 175$ cm^{-1} at 300 K) is nearly temperature independent, closely corresponding to the location of the anti-resonance dip in the Raman response of the coupled peaks. The coupling parameter Δ_{12} (figure 4(d)) progressively decreases, until, close to T_i where the dip between the two peaks virtually disappears, the CDHO fit becomes no longer justified, becoming equivalent to a fit with single damped harmonic oscillator. The strength of the lower peak vanishes at T_i, whereas neither frequency nor strength of the upper peak shows any noticeable discontinuity at the transition. Only its damping parameter rather abruptly increases on approaching T_i. Above this temperature, the frequency of the upper mode slightly hardens and its band shape continues to be well described by a broad but still underdamped oscillator—with a temperature factor of the first-order mode. We note that with appreciable damping at higher temperatures the fitted quasi-harmonic peak frequencies of broad peaks lie noticeably higher than the positions of the apparent peak maxima. This is due to increasing enhancement of the low-frequency wing of the Raman peak by the temperature factor—see figure 3(b).

The lowest-frequency feature x at 140 cm^{-1} seems to be completely decoupled from modes 1 and 2 all the way up to T_i; our attempts to use a CDHO model for all three lowest-frequency modes did not bring any improvement. In order to obtain its parameters, however, it could be satisfactorily fitted with a Gaussian profile—alternatively with first-order or second-order (overtone) temperature factor. It broadens with increasing temperature and its frequency progressively softens. This band could be reliably followed up to a few degrees below T_i, where its frequency dropped to below $\sim$50 cm^{-1} and the peak started to disappear in the Rayleigh wing (figure 1). Its integrated intensity shows anomalous temperature behaviour, irrespective of the type of temperature factor used.

Concerning the frequency region below 300 cm^{-1}, our results disagree with the behaviour reported by Scott [26, 27]. While our measurements confirm strong bilinear interaction between the two lowest first-order A_1 modes for all temperatures up to the transition, there is only very slight softening of their bare frequencies ω_1 and ω_2. The standard mode-coupling formulas describe quite accurately the coupled line shape observed by us. In particular, we did not observe any small satellite (a 'coupled two-phonon state') emerging at $\sim$145 cm^{-1} at temperatures approaching the phase transition, as reported in [26]. Instead, in our $A_1(zz)$ spectra we see an apparently uncoupled low-frequency feature growing in strength and strongly softening all the way from room temperature (140 cm^{-1}) up to T_i.

Our Raman spectra of figure 1 suggest an increase in the quasi-elastic scattering at temperatures close to T_i and higher, as manifested by a rise of the Rayleigh wing. This could be qualitatively simulated in the fits by central Gaussian component in the high-temperature spectra—see figure 3. The existence of quasi-elastic scattering was independently confirmed using a Brillouin set-up: in figure 5 we show the results of the temperature dependence of the quasi-elastic scattering in $AlPO_4$ measured in the $y(zz)x$ configuration.

4. Discussion

4.1. Coupling and fine structure of the low-frequency A_1 modes

As proposed in [26, 27], the origin of the coupling between the two lowest-frequency A_1 modes should be understood as due to anharmonic (third-order) indirect interaction of these modes via the two-phonon background. It was shown that a simple phenomenological Green-function treatment of this interaction by Ruvalds and Zawadowski [45, 46] could qualitatively reproduce the observed line shapes of the Raman response of the coupled modes. Generalizing slightly the model of [46] to include the inherent higher damping of the 221 cm^{-1} mode (due to

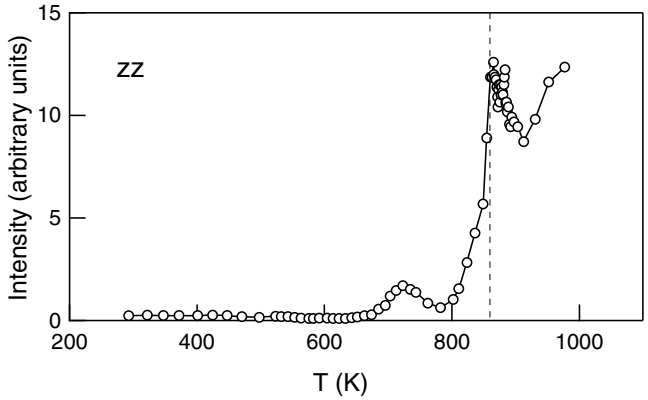

Figure 5. Temperature dependence of the quasi-elastic scattering in $AlPO_4$ in the $x(zz)y$ configuration. The phase transition temperature, $T_i = 860$ K, is marked by a dashed vertical line.

anharmonic interactions with other components of the two-phonon background) and tweaking its parameters, we could indeed obtain a fit to our spectra essentially identical to the simple CDHO quasi-harmonic mode coupling described above.

The decoupled mode parameters obtained from our CDHO fits describe those of a rather broad and strong higher-frequency mode, only slightly softening with increasing temperature, interacting with a narrow weaker mode, whose frequency is practically temperature independent and whose strength gradually decreases. The damping of the higher mode is approximately proportional to temperature up to about 50 K below T_i. It shows an abrupt increase and anomaly near T_i but no appreciable variation above (figure 4(b)). The damping and strength of the lower mode remain quite small up to T_i, where the mode becomes unobservable. Our choice of real coupling parameter, which vanishes at the transition, seems to be appropriate to the picture of two interacting modes, of which the lower one ceases to be Raman active at T_i because of the symmetry change at the phase transition.

As shown by Zawadowski and Ruvalds [46], their treatment can also describe the resonance enhancement of two-phonon states nearly degenerate with a single-phonon state, i.e. the Fermi-resonance type of interaction. In this sense, the additional fine structure observed on the line shape of the 221 cm^{-1} mode in our spectra at lower temperatures (cf figure 2(a)) can be possibly attributed to hybridization effects due to close coincidence of its frequency with that of singularities in the two-phonon density of states—namely two-phonon continua cut-offs. While, for practical reasons, we included the fine structure in our CDHO fits by means of additional independent peaks, we also verified that the model of [45, 46] is indeed able to describe both effects simultaneously. It can be straightforwardly generalized to include indirect coupling of an A_1 mode to another one via the two-phonon continuum as well as its hybridization with two-phonon states near a two-phonon cut-off frequency resulting in additional structure. With a suitable choice of parameters, one can obtain a reasonable description of the additional structure of the coupled line shape.

Among candidates for the requisite two-phonon cut-offs are, for instance, the branches connected with the two lowest E-symmetry modes located at $\sim$106 and 117 cm^{-1} at room temperature [12, 13]. As figure 2 shows, the frequencies of the fine-structure features indeed closely agree with overtones of these E modes. Although the underlying two-phonon cut-offs need not correspond to states at the Brillouin zone centre, the frequencies are not likely to be very different in view of the flatness of these 'E' branches as reported in neutron scattering

studies [14, 15]. It is also evident that the two-phonon states of E branches do have A_1-symmetry components to make the interaction with A_1 modes allowed.

4.2. Soft low-frequency feature in the α-phase

The lowest 140 cm^{-1} feature x, whose origin is not clear, deserves special attention. A somewhat similar 'soft' feature was reported in $AlPO_4$ by Scott [26, 27], who observed a peak emerging at 145 cm^{-1}, albeit only at rather high temperatures approaching the phase transitions. He assigned it to a coupled two-phonon state, resulting from interaction and assumed crossing of a softening A_1 mode (219 cm^{-1}) with a 'hard' two-phonon (2TA) band. This picture is based on an analogy with quartz, where the problem of explaining the additional soft low-frequency mode in the A_1 Raman spectra arose [47, 48].

Whereas, in our analysis, neither of the coupled A_1 modes discussed above shows appreciable softening of its bare frequency in the whole temperature range up to T_i, the lowest-frequency feature as observed by us softens considerably, remaining apparently uncoupled from the former two. Instead of 'a coupled two-phonon state' suggested in [26], we tentatively propose to interpret this feature as a manifestation of an inherently soft two-phonon state somewhere near the Brillouin zone boundary.

In α quartz, Boysen *et al* [49] did observe by inelastic neutron scattering a pronounced softening and coupling of the two lowest acoustic branches along the Γ-M direction; however, no analogous study in $AlPO_4$ has been reported so far. Although there are twice as many dispersion branches in $AlPO_4$ as in SiO_2 because of the doubled unit cell, the corresponding phonons in $AlPO_4$, especially for wavevectors perpendicular to the zone folding direction (c^*), are expected to have similar frequencies—in general slightly lower than in SiO_2 [14, 16]. The available neutron data (see table 3 and figure 3 of [14]) give for the frequencies of the three acoustic branches at the M point of $AlPO_4$ the following values: $\sim$62, 65 and 72 cm^{-1}. These frequencies correspond quite well to half the frequency (at 300 K) of our 'extra' mode. The flatness of the dispersion curves in the close vicinity of the M point [14] also suggests a high density of phonon states. Hence, we propose to ascribe the 'extra' Raman band to a purely second-order scattering by pairs of phonons with opposite wavevectors $\boldsymbol{q}$ originating from an inherently soft branch—probably acoustic—near the M point. The line widths and line shapes of second-order scattering are largely affected by the underlying two-phonon density of states (unlike the case of first-order scattering), because the participating phonon pairs do not come from a single point in the $\boldsymbol{q}$-space, but rather from a convolution of states connected by the momentum conservation condition $\boldsymbol{q}_1 + \boldsymbol{q}_2 \approx 0$. We believe that the observed anomalous temperature behaviour in the scattering strength of the lowest observed mode should be ascribed mainly to density-of-states effects of a softening phonon branch. The possibly expected structure due to van Hove singularities in the density of states is sufficiently smeared at not too low temperatures that a broad Gaussian multiplied by an appropriate second-order thermal factor $(1 + n(\frac{\omega}{2}, T))^2$ for overtone processes may give a suitable approximate description of the line shape.

In the absence of relevant data for $AlPO_4$, it is instructive to compare the temperature dependence of the frequency of our low-frequency soft mode x, as determined from our fits, with the second harmonic of the lowest 'acoustic' soft phonon modes from the M-point, as observed by Boysen *et al* in α-quartz (figure 2 in [49]). There is, indeed, a qualitative agreement in the temperature behaviour.

According to [49], the softening of the lowest 'acoustic' branch in the M point of α-SiO_2 results mainly from its coupling with the second lowest 'acoustic' branch. Let us note that dispersion curves reported in [14] indicate that the $AlPO_4$ analogue of this upper soft acoustic

branch (taking into account additional anti-crossings and eigenvector exchanges) seems to be connected with one of the two lowest doubly degenerate E(Γ)-modes (at 106 and 117 cm^{-1} at 300 K). Preliminary results of our Raman studies of the E modes (to be published elsewhere) also indicate quite appreciable softening of the second lowest E mode on heating.

4.3. The β phase

In agreement with the group theory predictions (table 1), only three A_1 modes are expected in the β phase. The remaining five change their symmetry to Raman inactive species B_1 (see table 1). Our results show that above T_i (at least over an interval of 200 K) there are *four* distinct Raman peaks (figure 1). Our detailed analysis further shows that all four modes behave like first-order phonon peaks over the whole investigated temperature range and that, on heating, their frequencies and strengths do not show noticeable discontinuities at the transition temperature.

By analogy to quartz [48], the lowest peak in β-$AlPO_4$ was attributed to second-order origin, resulting from an interaction and eigenvector exchange between the soft mode (the second lowest A_1 mode in the α phase) and a 'hard' two-phonon state from the zone boundary [26, 27]. This picture of the lowest peak as a mixed excitation gradually changing from the first-order soft mode at low temperatures to a second-order excitation at high temperatures is not based on any line shape analysis of rather crude Raman data; it relies on the assumption of hybridization due to interaction of a softening A_1 phonon with an unspecified temperature independent two-phonon state.

As in quartz, the structural change at the α–β transition corresponds to a rigid rotation and shift of all the AlO_4 and PO_4 tetrahedra in radial directions (along twofold axes). In the β phase, Al and P are fixed by symmetry in the Wyckoff positions (3c) and (3d), respectively, whereas the O atoms occupy general (12k) positions in the hexagonal primitive cell. Hence, we are left with three degrees of freedom, i.e. the (x, y, z) coordinates of oxygen atoms, giving rise just to three possible totally symmetric A_1 modes in this structure. The idea has been put forward several times [49–54] that the high-temperature β-quartz might be hexagonal only on average: i.e. not a static hexagonal structure, but due to dynamical microtwinning—coexistence of the two possible trigonal α-phase domain states (Dauphiné twins) on a microscopic scale. These two states, referred to as α_1 and α_2, are related by 180° rotation of the structure about the $\boldsymbol{c}$ axis and differ thus by the sign of the order parameter (chosen e.g. as the angle of rotation of the SiO_4 tetrahedra from the ideal β structure).

Invoking such an idea for the case of $AlPO_4$, we could imagine Al and P atoms shifted from the ideal β-phase positions corresponding to high-symmetry 3c and 3d Wyckoff sites and assume that they are dynamically disordered over the 6g and 6h sites of the hexagonal group ($P6_422$ or $P6_122$), respectively. The 6g and 6h sites correspond to the 3a and 3b sites of the trigonal group ($P3_121$ or $P3_221$). Without making any assumptions on the positions of oxygen atoms, which may be possibly disordered over positions of general symmetry (12k) to accommodate the shifts of Al and P by keeping the tetrahedra reasonably rigid, this idea would supply the 'missing' degree of freedom, namely the displacement of Al and P in the radial direction towards the trigonal sites. A symmetry analysis within the framework of the hexagonal 622 (D_6) factor group would yield in this case the following symmetry decomposition for the 51 Γ-point optical modes in the 'disordered' β phase:

$$\Gamma_{op} = 4A_1 + 4A_2 + 4B_1 + 5B_2 + 8E_1 + 9E_2.$$

Actually, the underlying assumption of this decomposition is that the disorder of Al and P over the 'trigonal' 6g and 6h sites is not completely random, but dynamically correlated in such a way as to maintain one of the two α-phase domain states on a local scale.

Compared with the standard result, $3A_1 + 4A_2 + 5B_1 + 5B_2 + 9E_1 + 8E_2$ (see table 1), the most important difference is that in the 'average' β phase of $AlPO_4$ we should indeed expect to observe four Raman active A_1 modes instead of three. Because of the lower site symmetry and concomitant disorder in Al and P sites, one of the A_1 modes is not transformed into B_1 species, retaining its Raman activity. Another subtler spectroscopic consequence of this idea follows from the exchange in the number of E_1 and E_2 optic modes in the β phase, since these have different selection rules for Raman scattering (cf table 1). However, this effect might be difficult to verify, in view of the vanishing strength of some of the E modes. We note that the consequences are meaningful as long as the average dwell time of the atoms in the individual trigonal positions is much longer than the corresponding inverse phonon frequency.

Support for our idea is given by a recent molecular dynamics simulation of the structural changes in $AlPO_4$ by Kihara and Matsui [25]. They find in the β phase a bimodal character of the probability distribution function of atoms—with Al and P atoms spending most of the time in the two equivalent 'trigonal' positions—and conclude that the structure change is rather of order–disorder regime, with trigonal-phase α_1 and α_2 clusters emerging below T_i and persisting at $T > T_i$. The x-ray structure study of $AlPO_4$ by Muraoka and Kihara [24] also shows that the vibrational amplitude of oxygen along one of the axes of the thermal ellipsoid, namely the direction joining the α_1 and α_2 positions, abruptly increases at the transition.

In this connection, let us recall the results of quasi-elastic scattering in $AlPO_4$ (figure 5). On approaching the transition, there is a steep rise in the scattering intensity with the onset at $\sim$800 K, where the quasi-elastic scattering intensity abruptly increases by about two orders of magnitude; it passes through a maximum at T_i and remains rather high above T_i (at least up to $\sim$1000 K, the highest investigated temperature). The 800–1000 K range in figure 5 can be schematically decomposed into two components: a peak centred on T_i (corresponding to the critical opalescence near a phase transition) superimposed on a broad rising edge, appearing in the vicinity of 800 K and increasing upon heating. In our opinion, the onset of the edge below T_i reflects the onset of local disorder in the α phase, and the high level of quasi-elastic scattering in the investigated range of temperatures above T_i would originate from the dynamical disorder of the β phase, as a consequence of the dynamical clustering or microtwinning suggested above. We point also to the fact that the damping anomalies of all the four strong A_1 modes set on at about the same temperature as the edge—approximately 50 K below T_i—see figure 3(b).

Interestingly, the onset in quasi-elastic scattering towards the transition is preceded by a well defined broad peak appearing at over 100 K below the transition. Lacking at present any satisfactory explanation of this 'pretransition' phenomenon, we merely note that the position of this peak correlates with a marked anomaly in the temperature dependence of the cation–anion distances in the PO_4 tetrahedra, as observed in [22, 23] (see also [16]). The Raman mode frequencies do not exhibit any noticeable anomalies in this temperature range (see figure 4(a)). One can then speculate about some smooth change taking place in the very long range order, but deeper investigations (such as small-angle x-ray scattering) are needed to understand this 'pretransition' signature.

5. Conclusion

Concluding, we propose to identify the 'extra' A_1 mode in the β phase with our first-order $\sim$200 cm^{-1} Raman mode, explaining thus its Raman activity persisting in the whole temperature range by the disordered nature of the β phase. Its virtually temperature independent strength indicates that its eigenvector—which mainly determines the Raman mode strength—is likely to depend on temperature only weakly. Since this A_1 mode should represent the 'rigid' tetrahedron mode in a double-well potential with minima at the equivalent 'trigonal'

α_1 and α_2 sites, its high damping in the 'β'-phase is consistent with its 'disordered' origin. Independent data from other methods are clearly desirable to support or dismiss this idea.

Acknowledgments

One of the authors (IG) thanks CNRS (*Département Sciences Chimiques*) for inviting him to a '*poste rouge*' position and CRMHT–CNRS in Orléans for hospitality. Fruitful discussion with Dr J Petzelt is gratefully acknowledged.

References

[1] Kosten K and Arnold H 1980 *Z. Kristallogr.* **152** 119
[2] Beck W R 1949 *J. Am. Ceram. Soc.* **32** 147
[3] Van Tendeloo G, Van Landuyt V and Amelinckx J 1976 *Phys. Status Solidi* a **33** 723
[4] Bachheimer J P, Berge B and Dolino G 1984 *Solid State Commun.* **51** 55
[5] Saint Grégoire P, Schäfer F J, Kleemann W, Durand J and Goiffon A 1984 *J. Phys. C: Solid State Phys.* **17** 1375 and references therein
[6] Lazarev A N, Mazhenov N A and Mirgorodskii A P 1979 *Opt. Spektrosk.* **46** 619 (Engl. transl. 1979 *Opt. Spectrosc. (USSR)* **46** 348)
[7] Lazarev A N, Mirgorodskii A P and Mazhenov N A 1980 *Vibrations of Oxide Lattices* (Leningrad: Nauka) pp 123–52 (in Russian)
[8] Kislovskii L D, Shternberg A A, Mironova G S, Zvereva O V, Zdobnikov A Y and Vasilev A B 1987 *Opt. Spektrosk.* **63** 114 (Engl. transl. 1987 *Opt. Spectrosc. (USSR)* **63** 65)
[9] Goullet A, Camassel J, Montaner A, Pascual J, Jumas J C and Philippot E 1988 *Phys. Scr.* **37** 395
[10] Goullet A, Camassel J, Martin L, Pascual J and Philippot E 1989 *Phys. Rev.* B **40** 5750
[11] Camassel J, Goullet A and Pascual J 1988 *Phys. Rev.* B **38** 8419
[12] Scott J F 1971 *Phys. Rev.* B **4** 1360
[13] Goullet A, Pascual J, Cusco R and Camassel J 1991 *Phys. Rev.* B **44** 9936
[14] Bethke J, Eckold G and Hahn T 1992 *J. Phys.: Condens. Matter* **4** 5537
[15] Mazhenov N A, Smirnov M B and Shchegolev B F 1992 *Opt. Spektrosk.* **72** 129 (Engl. transl. 1992 *Opt. Spectrosc. (USSR)* **72** 70)
[16] Schober H and Dorner B 1994 *J. Phys.: Condens. Matter* **6** 5551
[17] Ouillon R, Pinan-Lucarre J P and Ranson P 2000 *J. Raman Spectrosc.* **31** 605
[18] Jayaraman A, Wood D L and Maines R G Sr 1987 *Phys. Rev.* B **35** 8316
[19] Gillet P, Badro J, Varrel B and McMillan P F 1995 *Phys. Rev.* B **51** 11262
[20] Keskar N R, Chelikowsky J R and Wentzcovitch R M 1994 *Phys. Rev.* B **50** 9072
[21] Watson G W and Parker S C 1995 *Phys. Rev.* B **52** 13306
[22] Ng H N and Calvo C 1976 *Can. J. Phys.* **54** 638
[23] Lang R, Calvo C and Datars W R 1977 *Can. J. Phys.* **55** 1613
[24] Muraoka Y and Kihara K 1997 *Phys. Chem. Miner.* **24** 243
[25] Kihara K and Matsui M 1999 *Phys. Chem. Miner.* **26** 601
[26] Scott J F 1970 *Phys. Rev. Lett.* **24** 1107
[27] Scott J F 1974 *Rev. Mod. Phys.* **46** 83
[28] Magneron N, Luspin Y, Hauret G and Philippot E 1997 *J. Physique* I **7** 569
[29] Magneron N, Luspin Y, Hauret G and Philippot E 1998 *Eur. Phys. J.* B **3** 7
[30] Magneron N 1998 *Thesis* University of Orléans, unpublished
[31] Schwarzenbach D 1966 *Z. Kristallogr.* **123** 161
[32] Swanson H E, Cook M I, Evans E H and de Groot J H 1960 *Standard X-Ray Diffraction Powder Pattern* NBS Circular no 539, vol 10 (Washington, DC: US Government Printing Office) p 3
[33] Chang Z P and Barch G R 1976 *IEEE Trans. Sonics Ultrason.* **23** 127
[34] Goiffon A, Jumas J C, Avinens C and Philippot E 1987 *Rev. Chim. Miner.* **24** 593
[35] Jumas J C, Goiffon A, Capelle B, Zarka A, Doukhan J C, Schwartzel J, Détaint J and Philippot E 1987 *J. Cryst. Growth* **80** 133
[36] Philippot E, Goiffon A, Maurin M, Détaint J, Schwartzel J, Toudic Y, Capelle B and Zarka A 1990 *J. Cryst. Growth* **104** 713
[37] Porto S P S and Scott J F 1967 *Phys. Rev.* **157** 716

[38] Mirgorodskii A P 1980 *Opt. Spektrosk.* **48** 183 (Engl. transl. 1980 *Opt. Spectrosc. (USSR)* **48** 104)
[39] Barker A S and Hopfield J R 1964 *Phys. Rev.* A **135** 1732
[40] Katiar R S, Ryan J F and Scott J F 1971 *Phys. Rev.* B **4** 2635
[41] Gillet P, Le Cléac'h A and Madon M 1990 *J. Geophys. Res.–Solid Earth* **95** 21635
[42] Castex J and Madon M 1995 *Phys. Chem. Miner.* **22** 1
[43] Gervais F, Piriou B and Billard D 1975 *Solid State Commun.* **17** 861
[44] Gervais F 1976 *Ferroelectrics* **13** 555
[45] Ruvalds J and Zawadowski A 1970 *Phys. Rev.* B **2** 1172
[46] Zawadowski A and Ruvalds J 1970 *Phys. Rev. Lett.* **24** 1111
[47] Shapiro S M, O'Shea D C and Cummins H Z 1967 *Phys. Rev. Lett.* **19** 361
[48] Scott J F 1968 *Phys. Rev. Lett.* **21** 907
[49] Boysen H, Dorner B, Frey F and Grimm H 1980 *J. Phys. C: Solid State Phys.* **13** 6127
[50] Wright A F and Lehmann F S 1981 *J. Solid State Chem.* **36** 371
[51] Dolino G and Bastie P 1995 *Key Eng. Mater.* **101/102** 285
[52] Dolino G, Bachheimer J P, Gervais F and Wright A F 1983 *Bull. Minéral.* **106** 267
[53] Heaney P J and Veblen D R 1991 *Am. Mineral.* **76** 1018
[54] Smirnov M B and Mirgorodsky A P 1997 *Phys. Rev. Lett.* **78** 2413